# Fracture toughness of composite acrylic bone cements

J. PEREK, R. M. PILLIAR*
*Centre for Biomaterials, University of Toronto, 170 College Street W., Toronto, Ontario, Canada M45 1A1*

Composite bone cements incorporating one of four different filler particles (hydroxyapatite powder, graphite flakes or one of two types of rubber-modified acrylic particles) were made and the fracture toughness properties ($K_{Ic}$) and curing characteristics (peak curing temperature and cement extrudability while in the doughy state) assessed. The results showed that all filler types studied resulted in significant increases in fracture toughness while maintaining acceptable working and curing characteristics of the composite cements. The increase in $K_{Ic}$ was related to the amount of filler incorporation. The observed dependence of the change in $K_{Ic}$ on the wt% filler could be rationalized through the application of proposed mechanisms for toughening of particle-reinforced polymers.

## 1. Introduction

Numerous clinical studies have suggested deficiencies in the mechanical properties of currently used bone cement. Inadequate fracture resistance can lead to cement breakup and subsequent implant loosening [1, 2]. Although mechanical property improvement is possible through the incorporation of fibre-reinforcing phases, previous studies have shown that the flow characteristics of the resultant composite in its "doughy" state are severely compromised [3]. This has led to studies of particulate-filled composite bone cements that offer the possibility of improved mechanical properties without severe reductions in flow characteristics of the precured polymers [4]. This investigation explored this approach further through the incorporation of particulate fillers within low-viscosity bone cement. Our objective was to study the effect of different particulate fillers on the curing characteristics and fracture toughness properties of particulate-filled composite cements.

## 2. Experimental

### 2.1. Materials and sample preparation

A low-viscosity radio-opaque bone cement (Zimmer) was used with particulate fillers being added as described below. The as-received bone cement powder was divided into 5 g lots and 2.5 ml liquid monomer provided with the powder in the bone cement kit was added to each lot to form enough cement dough to make ten miniature short-rod fracture toughness test specimens. These were formed in Teflon moulds with multiple cavities (Fig. 1). The specimens consisted of cylinders 7 mm long and 4 mm in diameter with a 9.5 mm loading collar at one end [5, 6] (Fig. 2). The small test specimen size allowed a number of specimens with different fillers to be made using bone

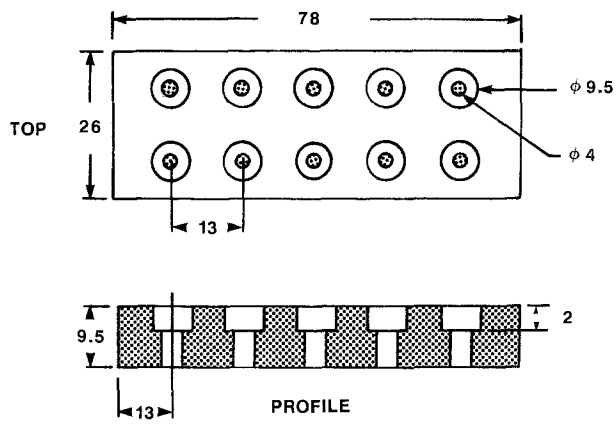


*Figure 1* Moulds for the preparation of specimen preforms.

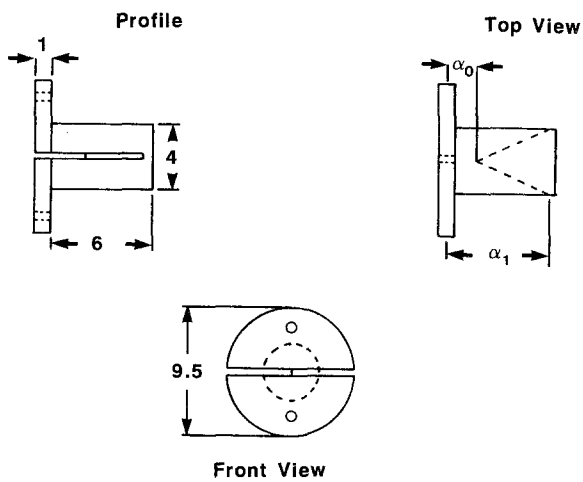


*Figure 2* Miniature short-rod fracture toughness test specimen geometry.

* Author to whom all correspondence should be addressed.

cement from a single bone cement kit. This eliminated concerns related to possible variations in composite cement properties attributable to differences in the cement matrix.

The bone cement components were blended in a stainless steel bowl in the specified ratio and mixed manually with a stainless steel spatula. After stirring for approximately 2 min, the entire cement bolus was transferred to a disposable plastic syringe (Monoject) and injected into the mould cavities. Teflon sheets were clamped on both sides of the mould, exerting an approximate pressure of 19 kPa during cement curing. The samples were allowed to cure for 15 min before removal from the moulds.

Two loading holes were drilled in the specimen collar using #56C HSS jobber bits and a hardened steel drill guide. Once these operations were completed, a chevron notch was cut along the sample mid-section using a 0.25 mm-thick diamond-impregnated wafering blade. For this operation the specimen was held securely in a brass pedestal which was bolted to a platform beneath the blade. The holding jig could be rotated 120° about its pivot point, thereby allowing the chevron to be cut with two coplanar passes of the specimen relative to the saw blade, first with the jig in one position and then with it rotated through 120°.

Before testing, samples were annealed in a Fisher Isotemp forced draft oven for 24 h at 70 °C. This annealing served to relieve any residual stresses arising from the chevron slotting operation. All samples were tested at least 1 week after moulding and 2 days after annealing.

## 2.2. Filler materials

Four particulate fillers were included in the study. These are listed in Table I: 10 μm (approximate) calcium hydroxyapatite ($Ca_{10}(PO_4)_6(OH)_2$) powder, graphite flakes about 190 μm across with an aspect ratio, $s \approx 64$, 60 μm (approximate) Plexiglas DR100 rubber-modified poly(methyl methacrylate) (PMMA) particles, and 9 μm (approximate) Paraloid KM334 rubber-modified acrylic particles. The rubber-modified PMMA contained spherical rubber particles with a three-stage "cored" structure consisting of an inner PMMA core surrounded by a crosslinked rubber shell of butylacrylate costyrene and an outer shell of PMMA. The DR100 pellets supplied by the manufacturer were cryogenically ground to a powder for mixing with the bone cement powder.

Composites were formed by replacing a portion of the PMMA powder component of the bone cement kit with the fillers. Blending of the powder mixture was accomplished using a custom-built mixing chamber with a rotational velocity of 30 r.p.m. Powders were mixed for 10 min, after which the blend was carefully removed from the chamber and transferred to storage vials. A 2:1 powder-to-liquid ratio as specified by the cement manufacturer was used when forming the composite cements, but the mass of powder included the PMMA and filler particles.

## 2.3. Fracture toughness testing

A variation of the short-rod method reported by Wang and Pilliar [5, 6] was used to assess the plane strain fracture toughness of the composite samples. A full development of the theory for short-rod fracture toughness testing can be found in [7]. The applicable equation for fracture toughness determination of specimens corresponding to elastic–plastic fracture mechanics (EPFM) conditions is

$$K_{Ic} = \frac{P_c Y_m^*}{WD^{1/2}} \left( \frac{1 + p}{1 - p} \right)^{1/2} \quad (1)$$

where $P_c$ is the peak load during the test, $D$ is the specimen diameter, $W$ is the specimen length and $Y_m^*$ is the minimum stress intensity factor coefficient. The non-linear behaviour of the polymer specimen is accounted for by calculating the plasticity factor $p$ from a load–mouth opening plot and incorporating it into the relationship for $K_{Ic}$ determination.

Barker's EPFM test method [7] requires the measurement of applied load and a displacement proportional to the crack mouth opening. Traditional clip-on displacement gauges could not be fitted readily to our miniature specimens, so a non-contact laser telemetric system (Zygo model 121) was used to measure the specimen mouth opening during testing. The unit consisted of a HeNe gas laser with a resolution of 0.001 mm, connected to an RS232 signal-conversion module.

A specialized loading fixture was designed to grip the miniature short-rod samples firmly for testing on an Instron universal testing machine. An exploded diagram of the fixture is presented in Fig. 3. A short-rod sample resided in matching recesses on each half of the jig, supported on steel pins which passed through holes on the sample loading collar. Two laser apertures were mounted on the front of the loading fixture to provide a precise target for the laser beam and to contribute an additional gripping force on the specimen loading collars. An assembly plate was used

TABLE I A listing of the various filler particles used for this study

| Material | Supplier | Particle diameter (μm) |
|---|---|---|
| Hydroxyapatite ceramic Wie-A-182D | Sterling Winthrop Institute | 9.7 |
| Graphite flakes | Cal Graphite Corporation | 192 ($s = 64$)[a] |
| Rubber-modified PMMA Plexiglas DR100 | Rohm & Haas | 60 |
| Rubber-modified acrylic Paraloid KM334 | Rohm & Haas | 9.0 |

[a] $s$, Aspect ratio.

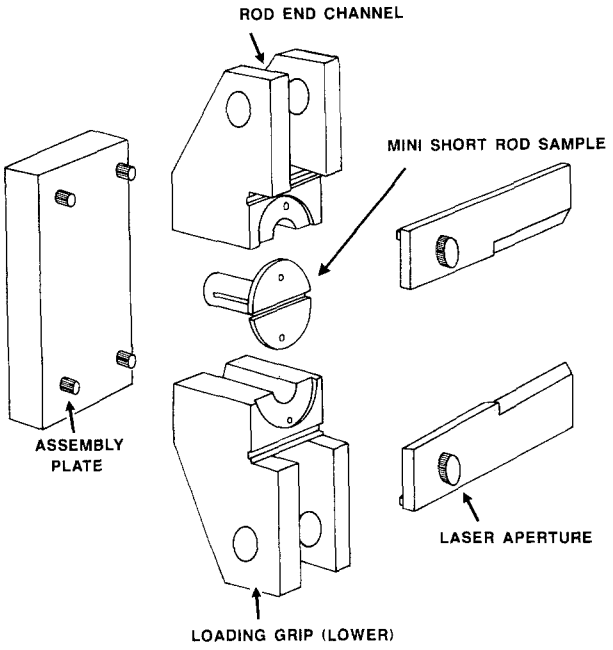


*Figure 3* Fracture toughness test specimen loading fixture.

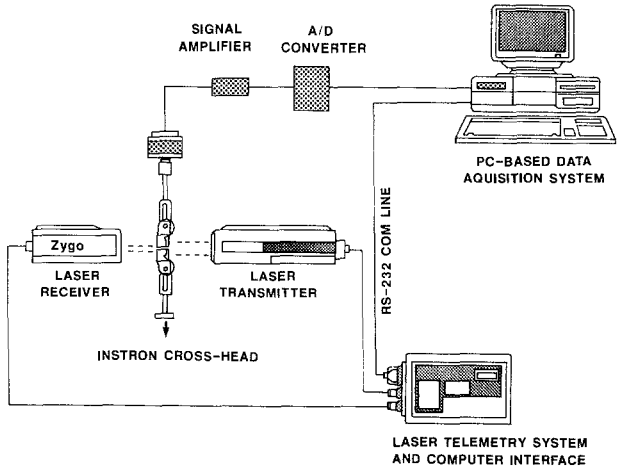


*Figure 4* Diagrammatic representation of data acquisition system for the determination of $K_{Ic}$.

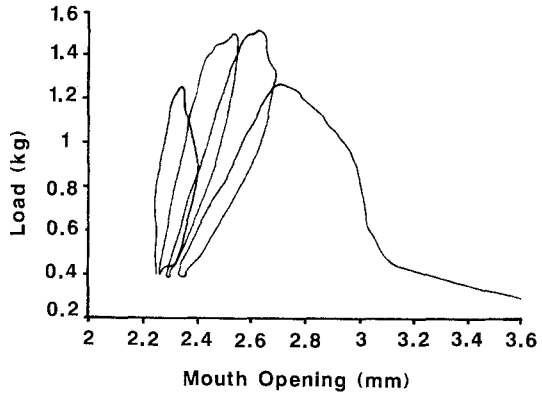


*Figure 5* Representative load versus mouth opening curve.

to assure proper alignment of the components and to protect the fragile short-rod specimen from unintentional loading when the fixture was being positioned in the tensile testing machine.

Specimens were loaded using an Instron TT-CM universal testing machine. The sample fixture was linked to the Instron via two connection rods fitted with MW series female rod ends (Rod Ends Mechanical Ltd, Toronto). These allowed the specimen to self-align during loading. The laser unit was bolted firmly to the loading frame and aligned so that the beam was incident on the middle section (approximately) of the aperture.

A simplified diagram of the data acquisition system is shown in Fig. 4. The system was controlled by an IBM PC-XT microcomputer which simultaneously collected data from the 50 kg load cell and the laser telemetric system. The output of the load cell was rerouted to a custom-built signal amplifier/filter unit and Contect ADC-30 analogue–digital converter card. The ADC-30 possesses a resolution of 12 bits and a conversion accuracy of $\pm$ 0.004% of full-scale range (at 25 °C).

The laser telemetry control unit automatically converted the displacement measured by the laser receiver to an RS232C signal that was compatible with the basic I/O board of the PC. The data acquisition program collected load–displacement–time data at a rate of 3 samples $s^{-1}$ and stored it on the hard disk of the PC using comma-delimited ASCII files. After proper vertical alignment of the jig and connecting rods on the loading frame, the assembly plate was removed. A crosshead speed of 0.05 cm $min^{-1}$ was selected for all tests.

Once a sample had been loaded to about half of its ultimate strength, it was subjected to three unload–reload cycles before loading to failure. These unload–reload operations were used to estimate the sample plasticity factor. The criterion for selecting the location of the unloading points was that attainment of the peak load must occur between two of the unload–reload operations [5–7]. A representative load–opening record is shown in Fig. 5. A typical test lasted approximately 10 min, during which time at least 800 data-points were collected. All tests were conducted at room temperature (23.3 $\pm$ 1.1 °C) in air. Fractured specimens were examined to determine the exact short-rod specimen dimensions and chevron notch geometry. This was accomplished by employing a Mitsutoyo toolmaker's microscope (model TM-201) equipped with digital micrometers accurate to 0.001 mm.

Due to the accurate estimation and interpolation procedures required to calculate $K_{Ic}$ from the load–opening test plots, a computer program was developed to complete the numerical analysis. The program calculated tangents to each of the four reloading curves on a load–mouth opening displacement graph and thereby estimated the mean sample plasticity factor. For this specimen geometry the peak load was defined as the point corresponding to the intersection of a line of slope equal to 0.45 of the initial loading slope with the load–displacement curve. Through compliance calibration experiments, Wang and Pilliar [5] found that $Y_m^*$ had a mean value of 25.0 for a sample with dimensions similar to those used in this

study. Consequently, this value was adopted for the analyses with a correction factor introduced to account for slight differences in the chevron geometry. The relationship for correcting $Y^*_m$ as described by Barker [7] is

$$Y^*_{m(corrected)} = 25.0(\alpha_1 - \alpha_0/0.950 - \alpha_0)^{1/2} \quad (2)$$

where $\alpha_1$ ($= a_1/W$) and $\alpha_0$ ($= a_0/W$) are dimensionless crack lengths. Fracture toughness values were calculated directly from the values of $Y^*_m$, $P_c$, $p$ and the specimen dimensions, using Equation 1.

## 2.3. Curing studies

In order to assess the effect of the various fillers on the maximum curing temperature, the temperature–time response of several polymerizing cements was investigated. Temperature probes consisted of $8 \times 10^{-2}$ mm diameter type-E (Ni–10% Cr/Co) duplex thermocouple wire (Omega Engineering Ltd). The probe end of the wire was spot-welded to form a bead and the other end was connected to the signal conditioner linked with the PC data acquisition unit. An ice-bath reference was utilized for all of the experiments.

The cements were polymerized in Teflon moulds identical to those used to cast the fracture toughness specimens. The temperature probe was inserted about 4 mm into the centre of the dough, using a tapered plastic alignment tube attached to a rigid bracket assembly (Fig. 6).

The data acquisition program measured the temperature at a given time received from the analogue–digital card and plotted the profile on the monitor. Data were stored in comma-delimited ASCII files at a rate of one sample every 4 s.

## 2.5. Calorimetric analysis

As an extension of the thermocouple tests, a calorimetric analysis was performed on the unmodified bone cement and filler powders to evaluate their specific heat capacity. The device employed was a Dupont 910 differential scanning calorimeter interfaced with a Dupont 9600 computer data acquisition and control unit. All data analysis was performed by the General 2.2 software package on a 9600 computer.

## 2.6. Workability (flowability) tests

Several of the modified cements which demonstrated high fracture toughness were evaluated for dough "flowability" to assess the effect of the fillers on the polymer rheology. The intrusion properties of these cements were assessed using procedures outlined in American Society for Testing and Materials standard F451 (Standard Specifications for Acrylic Bone Cements) [8]. An extrusion mould was fabricated from Teflon as outlined in the specification, and consisted of a die with four 1 mm diameter holes in its base and a cylindrical ram.

Bone cement compounds composed of 20 g powder to 10 ml liquid monomer were mixed as outlined above and transferred to the die cavity. Curing dough

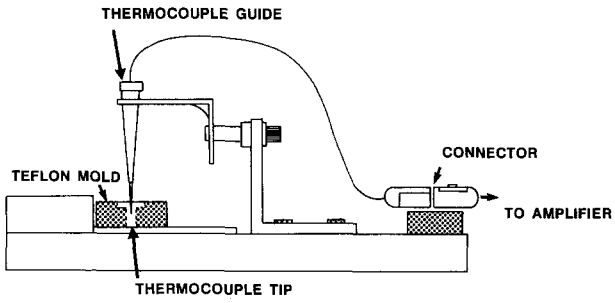


*Figure 6* Schematic representation of the experimental set-up for the measurement of temperatures during cement curing.

was forced through the holes in the base of the die by a weight placed on the ram. The lengths of the polymer strands discharged from each of the die holes were measured, and the figures averaged to yield a number proportional to the workability (flowability) of the cement.

## 2.7. Porosity determination

The percentage aerial porosity was calculated for two fractured short-rod controls, as well as for two fractured 40 wt % DR100 composites. The calculations were performed using a Perspective Systems Inc. digital image analysis system. Both halves of each specimen were mounted "face-up" in dental stone, and then ground down slightly to produce a flat examination area as close as possible to the actual fracture plane. A vaseline–lamp black mixture was rubbed on the polished surface, and the excess was carefully wiped away. This increased the contrast between the pores and the bulk polymer, simplifying the digitizing procedure. The porosity content was estimated by dividing the integrated pore area by the area of the examination region.

## 2.8. Fractography

Select samples from each subgroup were glued to pedestals (chevron surface up) and gold-coated for scanning electron microscopy (SEM) examination. A Hitachi S-520 scanning electron microscope was employed for all studies.

# 3. Results

## 3.1. Fracture toughness of modified bone cements

A complete synopsis of the experimental data can be found in Table II. Test data were subjected to an analysis of variance (ANOVA) study. The results of the statistical testing are summarized in Fig. 7.

Except for the 10 wt % DR100 and 1 wt % graphite cements, statistical analysis showed that all composites were tougher ($p < 0.005$) than unfilled control specimens. The variation in fracture toughness with wt % filler for each composite system is shown in Figs 8–11. All composites showed an increase in fracture toughness with increasing filler content over

TABLE II A summary of fracture toughness test data for each of the modified bone cements. The matrix for each system was Zimmer LVC cement

| Filler | wt % | vol %[a] | Plasticity factor | $K_{Ic}$ (MPa $m^{1/2}$) |
|---|---|---|---|---|
| Graphite flakes | 1 | 0.6 | 1.16 ± 0.05 | 1.13 ± 0.03 |
| Graphite flakes | 2 | 1.2 | 1.22 ± 0.07 | 1.26 ± 0.12 |
| Graphite flakes | 3 | 1.8 | 1.35 ± 0.22 | 1.34 ± 0.14 |
| Graphite flakes | 4 | 2.4 | 1.25 ± 0.12 | 1.43 ± 0.13 |
| Graphite flakes | 5 | 3.0 | 1.19 ± 0.04 | 1.34 ± 0.07 |
| Hydroxyapatite | 10 | 3.6 | 1.13 ± 0.09 | 1.23 ± 0.07 |
| Hydroxyapatite | 20 | 7.7 | 1.15 ± 0.05 | 1.23 ± 0.09 |
| Hydroxyapatite | 30 | 12.3 | 1.20 ± 0.08 | 1.33 ± 0.10 |
| Hydroxyapatite | 40 | 17.8 | 1.25 ± 0.07 | 1.55 ± 0.13 |
| Paraloid KM334 | 4 | 9.2 | 1.20 ± 0.09 | 1.43 ± 0.13 |
| Paraloid KM334 | 6 | 13.4 | 1.23 ± 0.13 | 1.74 ± 0.10 |
| Paraloid KM334 | 8 | 17.4 | 1.20 ± 0.06 | 1.48 ± 0.04 |
| Paraloid KM334 | 10 | 21.1 | 1.22 ± 0.09 | 1.55 ± 0.15 |
| Plexiglas DR100 | 10 | 9.5 | 1.15 ± 0.07 | 1.11 ± 0.10 |
| Plexiglas DR100 | 20 | 18.9 | 1.23 ± 0.14 | 1.37 ± 0.18 |
| Plexiglas DR100 | 30 | 28.3 | 1.27 ± 0.09 | 1.39 ± 0.07 |
| Plexiglas DR100 | 40 | 37.7 | 1.40 ± 0.06 | 2.08 ± 0.15 |
| Controls: Zimmer LVC mini short rods | | | 1.13 ± 0.07 | 1.07 ± 0.08 |

[a] Calculated values using known densities.

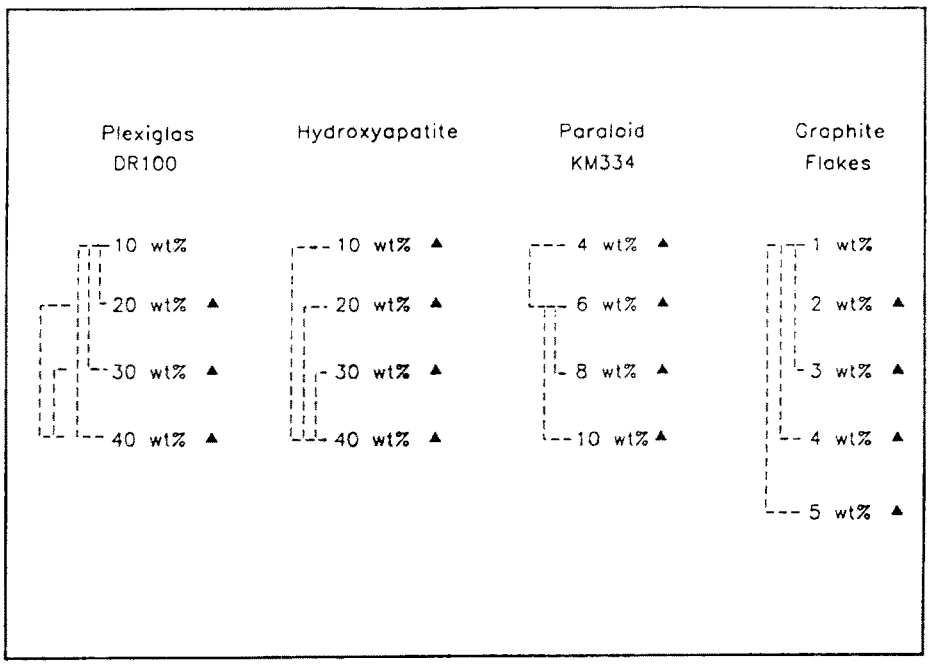


*Figure 7* Schematic summary of the ANOVA results for fracture toughness of the composite bone cements studied. (▲) Significant difference from Zimmer LVC controls at 99.5% and (---) significant difference between subgroups at 99.5%.

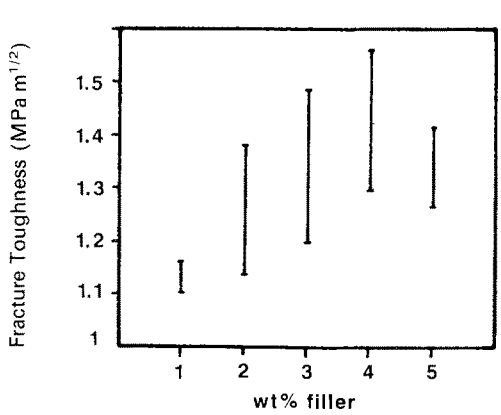


*Figure 8* Fracture toughness versus wt % graphite flakes.

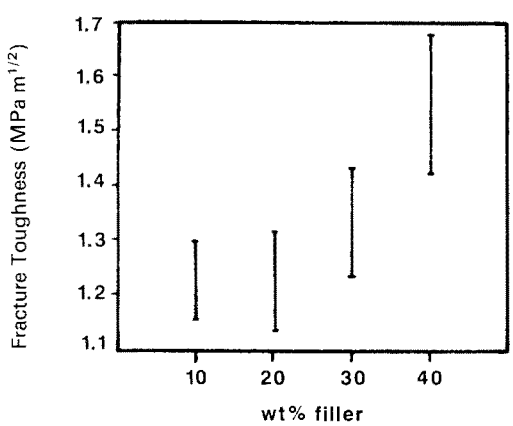


*Figure 9* Fracture toughness versus wt % Paraloid KM334.

the range studied, but to different degrees. Although an optimum filler content was suggested for the graphite flake and Paraloid KM334 rubber particles, this was not confirmed by statistical analysis. Further studies involving a wider range of filler volume fractions would be useful.

For the Plexiglas DR100-modified (Fig. 10) and the hydroxyapatite-modified bone cements (Fig. 11), the fracture toughness appeared to increase monotonically with filler content, at least over the range studied. Composite bone cements containing Plexiglas DR100 particles possessed the highest fracture toughness, $2.08 \pm 0.15$ MPa $m^{1/2}$. This coincided with the highest plasticity factor, $p = 1.40 \pm 0.06$.

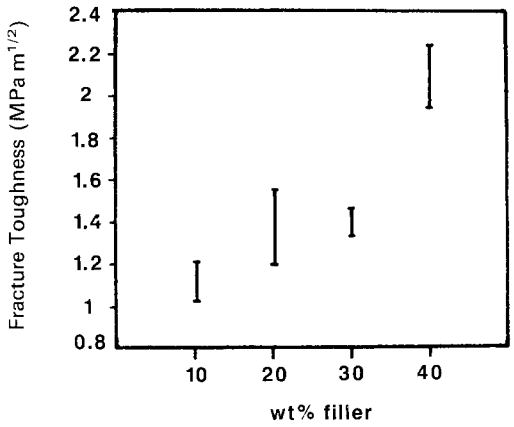


*Figure 11* Fracture toughness versus wt % hydroxyapatite.

## 3.2. Curing studies

A temperature profile for one of the unfilled cements is shown in Fig. 12. Table III summarizes the curing data for all of the composite systems. The unfilled control specimens produced the highest peak exotherm temperature during curing ($33.05 \pm 1.38$ °C) compared with all of the composite cements. In addition, the setting time was extended by incorporation of the fillers.

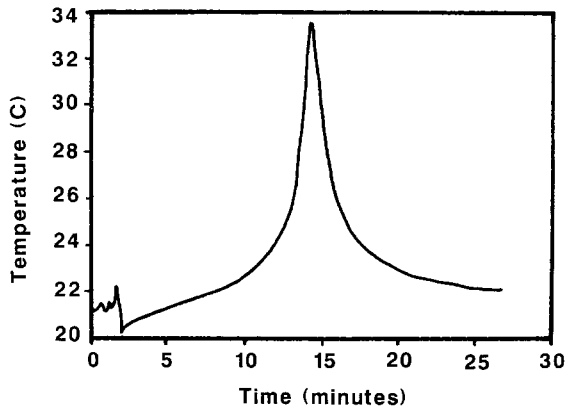


*Figure 12* Curing temperature profile for unfilled acrylic bone cements.

## 3.3. Calorimetric analysis

The results of the differential scanning calorimetry experiments are presented in Table IV. Heat capacity values were approximately constant over the temperature range of interest (25–35 °C). For each filler the heat capacity was less than that of unmodified bone cement, particularly for the graphite flake- and hydroxyapatite-filled cements.

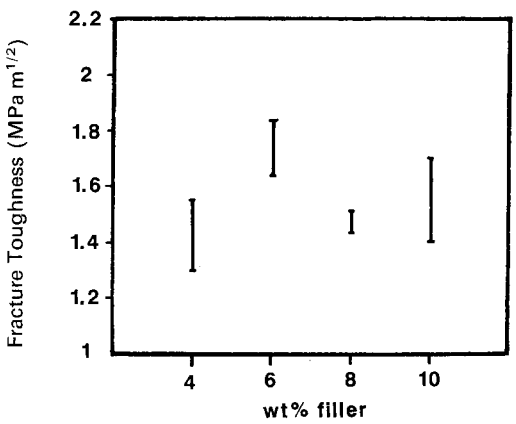


*Figure 10* Fracture toughness versus wt % Plexiglas DR100.

## 3.4. Workability studies

A summary of results from the workability trials is presented in Table V. Only the composite cement composition corresponding to the highest toughness measurement from each system was assessed for intrusion characteristics.

The only filled cement that exhibited superior intrusion properties to the unfilled low-viscosity cement was the 40 wt % hydroxyapatite composite. Both the 4 wt % graphite- and 6 wt % Paraloid-containing composite cements possessed intrusion characteristics only marginally inferior to those of the control sample. However, the cement containing 40 wt % Plexiglas DR100 demonstrated significantly lower workability characteristics (as defined by this test).

## 3.5. Porosity content

The two unfilled control samples had aerial porosity contents of 7.8 and 7.9%. In addition, the 40 wt %

TABLE III Data from the curing tests on representative composite cements

| Sample | Mass (g) | Peak temperature (°C) | Setting time (min) |
|---|---|---|---|
| 4 wt % Graphite | $0.27 \pm 0.02$ | $27.92 \pm 0.59$ | $13.68 \pm 0.28$ |
| 40 wt % Hydroxyapatite | $0.34 \pm 0.01$ | $25.86 \pm 0.46$ | $22.36 \pm 1.07$ |
| 6 wt % KM334 | $0.26 \pm 0.01$ | $27.38 \pm 1.48$ | $18.12 \pm 1.11$ |
| 40 wt % DR100 | $0.30 \pm 0.02$ | $24.89 \pm 0.82$ | $11.95 \pm 1.12$ |
| Zimmer LVC control | $0.27 \pm 0.03$ | $33.05 \pm 1.38$ | $7.60 \pm 1.05$ |

TABLE IV A summary of the heat capacity data for the particulate fillers determined by differential scanning calorimetry

| Material | Sample mass (mg) | Heat capacity ($J\,g^{-1}\,°C^{-1}$) |
|---|---|---|
| Sapphire reference | 61.6 | 0.79 |
| Zimmer LVC cement | 7.2 | 1.59 |
| Graphite flakes | 7.0 | 0.86 |
| Hydroxyapatite | 16.6 | 0.84 |
| Paraloid KM334 | 15.5 | 1.27 |
| Plexiglas DR100 | 16.3 | 1.45 |

TABLE V Results of the workability tests of the composite bone cements

| Material | Mean extrudate length (mm) |
|---|---|
| Zimmer LVC control samples | $13.8 \pm 0.8$ |
| Zimmer LVC + 4 wt % graphite flakes | $11.9 \pm 1.0$ |
| Zimmer LVC + 40 wt % hydroxyapatite | $15.0 \pm 1.1$ |
| Zimmer LVC + 6 wt % Paraloid KM334 | $12.4 \pm 0.4$ |
| Zimmer LVC + 40 wt % Plexiglas DR100 | $5.1 \pm 1.5$ |

DR100-containing composite was examined for porosity since it possessed the highest fracture toughness. Two of these specimens were analysed to yield porosity contents of 8.7 and 7.6%, suggesting that the inclusion of the particulate filler did not affect the sample porosity significantly.

### 3.6. Fractography

SEM micrographs of fracture surfaces for some composite bone cements are shown in Figs 13–16. Fig. 13 is a fracture surface of a graphite-reinforced cement, depicting two slots where graphite flakes were pulled out of the matrix during failure. In addition, the remains of a broken flake can be found in the top right-hand corner of the figure.

Fig. 14 shows a Paraloid KM334 composite cement, indicating significant ductile deformation during loading. The filler particles appear almost perfectly spherical and weakly bonded to the bone cement matrix.

Fig. 15 depicts the fracture surface of a cement modified with Plexiglas DR100, showing so-called river patterns (indicative of a brittle fracture) along the filler fracture surface, as well as numerous microvoids in the matrix. Remains of a fractured DR100 particle are evident in the centre. The filler particle appears to be well bonded to the bone cement matrix.

Fig. 16 illustrates the rough surface topography of a fractured hydroxyapatite-modified cement.

## 4. Discussion

### 4.1. Fracture toughness data

In general, a standard deviation of $\pm 10\%$ is considered to be very good for fracture toughness data from polymer specimens, a value of $\pm 40\%$ being more common [9]. For the unmodified Zimmer LVC control samples of the present study, the value of $K_{Ic}$ was $1.07 \pm 0.08\ MPa\,m^{1/2}$, a standard deviation of only $\pm 7.5\%$. Table VI compares this figure with others in the literature. Our value correlates well with those determined by other investigators using various testing methods.

If plane strain conditions are not maintained during testing, as might be the case with specimens of small cross-sectional area, unusually high $K_{Ic}$ values as a result of excessive crack-tip plastic deformation would be expected. It is worth noting that the $K_{Ic}$ values from this study correspond to the lower range of literature

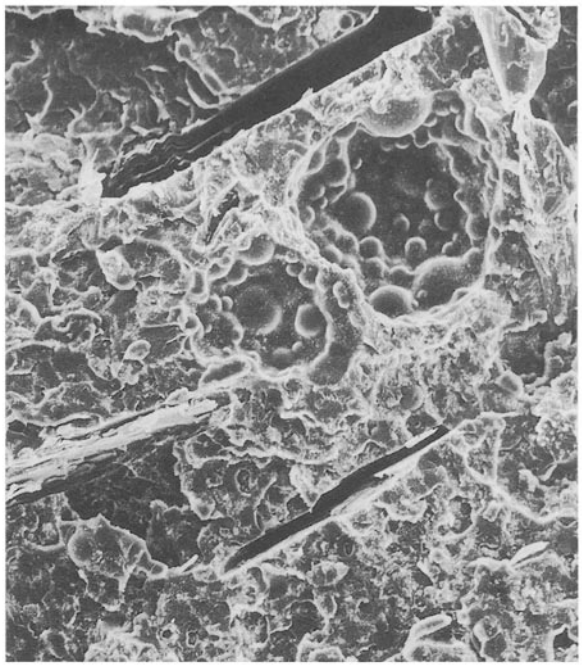

*Figure 13* SEM of the fracture surface of graphite composite cement. The slots represent regions from which graphite flakes have been pulled out during failure (× 115).

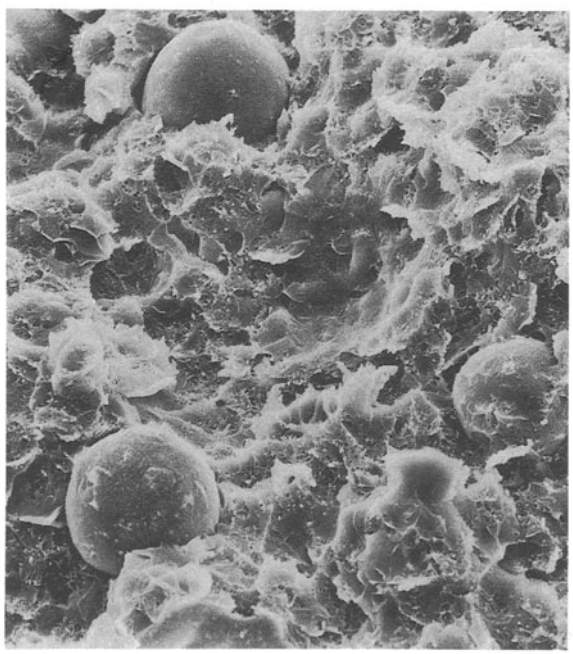

*Figure 14* SEM showing several Paraloid KM334 rubber particles at the fracture surface of a 6 wt % composite cement (× 280).

*Figure 15* Ductile pullout region near a filler particle on the fracture surface of a 20 wt % Plexiglas DR100 composite cement (× 115).

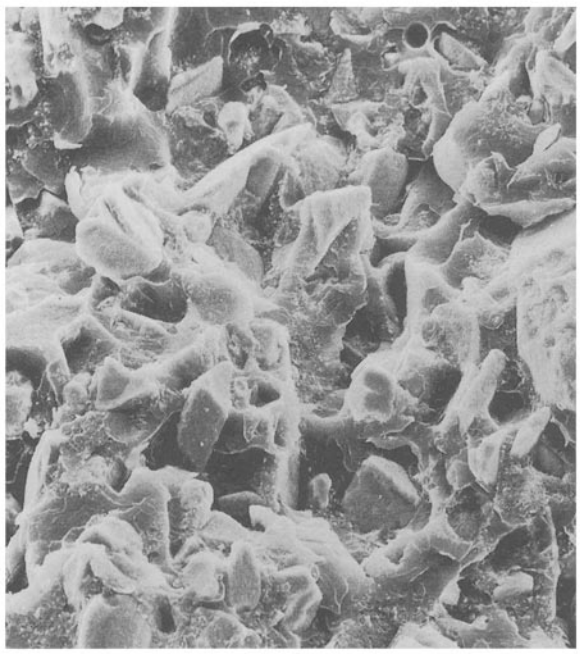

*Figure 16* Hydroxyapatite ceramic particles at the fracture surface of a 40 wt % composite bone cement (× 384)

TABLE VI A comparison of fracture toughness values for bone cement from the literature

| Reference | Cement | Mean $K_{Ic}$ (MPa $m^{1/2}$) |
|---|---|---|
| [6] | Zimmer LVC | 1.00 |
| [6] | Simplex-P | 1.01 |
| [10] | Zimmer regular | 1.42 |
| [10] | Zimmer LVC | 1.23 |
| [29] | Zimmer regular | 1.03 |
| Present study | Zimmer LVC | 1.07 |

values. This appears to support the validity of the miniature short-rod test method and the assumption of plane strain deformation.

The performance of the four composite bone cements developed in this study can best be determined by comparison with several modified cements from the literature. Robinson *et al.* [10] reinforced Zimmer regular and Zimmer LVC cement with 2 vol % graphite fibres, and found the fracture toughness to be 1.88 and 1.61 MPa $m^{1/2}$ respectively. Three other studies investigated the properties of PMMA reinforced with 7 wt % Kevlar-29 aramid fibres. Fracture toughness values of 2.61 MPa $m^{1/2}$ [11], 2.85 MPa $m^{1/2}$ [12] and 2.85 MPa $m^{1/2}$ [13] were reported. In addition, Pourdeyhimi and Wagner [11] utilized ultra-high molecular weight polyethylene (UHMWPE) fibres to modify the toughness of an unspecified bone cement. They found that 4 wt % fibres resulted in a composite cement with a fracture toughness of 1.86 MPa $m^{1/2}$

Several investigators elected to utilize rubber particles instead of fibres as reinforcing phases. Milios *et al.* [14] and Hooley *et al.* [3] both obtained fracture toughness values of 2.7 MPa $m^{1/2}$ for PMMA modified with 20 and 23 wt % rubber particles, respectively. In another study, Murakami *et al.* [15] found that CMW cement containing 30% rubber particles had a toughness of 2.26 MPa $m^{1/2}$

The only composite bone cement from this study that possessed a fracture toughness approaching the above values was the cement modified with DR100 rubber-modified PMMA particles. The cement containing 40 wt % DR100 exhibited a fracture toughness of 2.08 MPa $m^{1/2}$ By optimizing the cryogenic grinding process for DR100, it should be possible to produce a finer particle size and tighter size distribution. This will allow greater amounts of DR100 to be incorporated into the bone cement matrix, which may result in further toughening. The cement reinforced with 8 wt % Paraloid KM334 possessed a fracture toughness of 1.75 MPa $m^{1/2}$, making it similar to the cements modified with graphite or UHMWPE fibres.

There are several mechanisms that can be responsible for toughening in particle-reinforced polymers. First, the particles can effectively pin the crack front, necessitating a greater energy input before crack propagation can proceed. In an argument analogous to the pinning of dislocations, the crack front bows outwards between two rigid particles before breaking free [16]. The crack front elongates as it bows out, absorbing fracture energy. Work must be done by external forces to increase the crack length and to create the new crack surfaces. An expression for the effective fracture energy in such a case is [16]

$$G \approx G_m + T/d \quad (3)$$

where $T$ is the crack line tension, $d$ is the interparticle spacing and $G_m$ is the work of fracture for unmodified matrix. Note that a reduction in the interparticle spacing induces a corresponding increase in the fracture energy.

Separation of a well-bonded filler from the matrix material also requires energy input. As the advancing

crack plane intersects filler particles, further opening of the crack mouth demands that additional energy be provided to separate the filler–matrix interfaces. Consequently, poorly bonded fillers such as the graphite flakes and the hydroxyapatite particles of this study, cannot contribute effectively to toughening through this mechanism. If the filler–matrix interface is stronger than the filler itself, failure of filler particles will coincide with crack advancement. By transferring stresses from the matrix to an appropriate reinforcing phase, a considerable increase in fracture resistance can be realized.

One of the principal toughening mechanisms in polymers is crazing. Crazes are regions of numerous minute voids that develop in a plane normal to the applied load due to concentrated stresses [17, 18]. Coalescence of the voids is precluded by fibrils of oriented polymer which span the developing gap. Consequently, the existence of physical crosslinks or "entanglements" between chains is essential [19] to stabilize each fibril. Scission of the main-chain C–C bonds results in fracture of the fibrils, followed by development of a fissure due to void coalescence. This fissure extends along the craze centre to produce a crack.

Therefore, an increase in the craze density will effect a significant change in toughness because it translates to a greater absorption of fracture energy. For example, the work required to stretch crazes at the crack tip to the breaking point is given by [20]

$$G_{Ic} = NE_b L_0 \sigma_0 \quad (4)$$

where $N$ is the number of crazes, $E_b$ is the total strain in each craze at failure, $L_0$ is the length of polymer transformed to craze and $\sigma_0$ is the average stress for the entire deformation process. The variables $E_b$ and $L_0$ are functions of the type of polymer, and therefore can be considered constants. Consequently, the proportion of fracture energy absorbed by the crazing process is simply a linear function of the number of crazes nucleated. Crazing would occur preferentially at high-stress regions and this would correspond to the filler–matrix interface regions. Hence, an increase in filler content within a limiting range dictated by stress field interactions should result in increased crazing and fracture toughness, as was observed.

A fundamental mechanism of toughening is crack-tip blunting. Material at the crack tip which deforms plastically reduces the stress intensity and hence decreases the driving force for crack extension. Interaction between relatively soft rubber fillers, for example, and the crack front results in plastic deformation of the filler and hence a reduction in the crack-tip radius. In addition, interaction between the crack front and crazes emanating from the filler particle–matrix interface zone can reduce the crack-tip radius.

The cements reinforced with KM334 rubber-modified acrylic particles illustrated impressive gains in toughness with small additions of filler. With only 4 wt % KM334, $K_{Ic}$ increased from 1.07 MPa $m^{1/2}$ (control) to 1.43 MPa $m^{1/2}$. The largest improvement in toughness occurred at the 6 wt % level, where a $K_{Ic}$ of 1.74 MPa $m^{1/2}$ was determined. The fracture toughness appeared to drop slightly at 8 wt %, but the difference between the 8 and the 10 wt % values was not statistically significant.

SEM micrographs revealed several KM334 particles that had been slightly elongated during failure. Poor particle–matrix bonding presumably resulted in limited load transfer to the KM334 particles. Most of the particles observed were partially embedded within the matrix after failure, surrounded by a large number of dimples and ductile tears. Significant stress whitening was evident over the fracture surface, which indicated that extensive crazing had occurred. Therefore, the improved toughness for this composite can be attributed to crazing which initiated at stress concentrations at the filler particle–matrix interface as well as deformation of the filler particles.

The most impressive gains in toughness were achieved as a result of the DR100 filler particles. Additions of 10 wt % DR100 resulted in a fracture toughness of 1.11 MPa $m^{1/2}$, only marginally superior to that of unmodified Zimmer LVC. However, increasing the filler content to 20 wt % elevated $K_{Ic}$ to 1.37 MPa $m^{1/2}$. Shah [21] also found that the first signs of ductility in rubber-toughened PMMA occurred at 20 wt % filler. Another large increase was discovered at the 40 wt % level, where a $K_{Ic}$ of 2.08 MPa $m^{1/2}$ was measured.

SEM examination indicated a significant degree of bonding between the DR100 particles and the PMMA matrix. Ruptured DR100 particles on the fracture surface suggest that a substantial load was transferred to the filler before failure. This accounts for the superior toughness of this material compared with the other composites tested. Considerable stress whitening was visible on the fracture surface, which indicated that crazing contributed to the improved toughness. This suggests that significant toughness improvement is dependent on the filler being partly soluble in the matrix so that an interfacial bond can form while retaining the discrete nature of the particle.

The reinforcing agent should have superior mechanical properties to the matrix for the composite to demonstrate increased toughness. By employing a simple modelling technique, Rao [22] developed an empirical equation for the effective fracture toughness of a composite material, which was supported by tests on concrete. If $K_{1c}$ is the toughness of the matrix phase and $K_{2c}$ the toughness of the filler, then the effective fracture toughness $K_c^*$ of the composite can be expressed as [22]

$$K_c^* = (K_{1c} - K_{2c})(1 - V_f)^{0.5} + K_{2c} \quad (5)$$

where $V_f$ is the volume fraction of filler. For this simplified development, the value of $K_c^*$ appears to be solely dependent on the amount of reinforcement ($V_f$) and the fracture toughness of the constituent phases. However, several critical parameters are not considered in this expression, such as the degree of interfacial bonding, the relative elastic moduli of the two phases and the thermal expansion mismatch. Note

that Equation 5 states that an improvement in toughness is realized only through the addition of a tougher reinforcing phase.

Both graphite and hydroxyapatite are brittle materials capable of negligible plastic deformation, and are susceptible to sudden catastrophic failure during loading. According to the above argument, the composite cements containing these fillers should have shown a negligible improvement in fracture toughness. However, these modified cements exhibited significant increases in toughness compared with the Zimmer LVC control samples.

The $K_{Ic}$ of the graphite-modified cements increased with filler content to a maximum value of 1.43 MPa $m^{1/2}$ at 4 wt %. For the 5 wt% samples a slight decrease in toughness was exhibited, but the lack of further data points prevented us from determining whether the trend continued with greater additions. The improvement in fracture toughness can be attributed to a rise in the work of fracture due to contributions from platelet pullout work. SEM micrographs of the graphite composites suggest that minimal bonding had developed between the flakes and the bone cement. Consequently, the matrix was not able to transfer sufficient stress to the flakes to result in their fracture. Microscopy did reveal numerous slots on the fracture surface where flakes had obviously been pulled from the matrix during opening of the short rod. The contribution of pullout work to the work of fracture ($G_{pp}$) was defined by Piggott [23] to be

$$G_{pp} = V_p t \tau_i s^2/12 \quad (6)$$

where $t$ is the platelet thickness, $\tau_i$ is the interfacial shear stress and $s$ is the aspect ratio. As the crack mouth opens, flakes oriented perpendicular to the crack plane are pulled out of the matrix. The energy required to overcome the frictional forces at the flake–matrix interface increases the work of fracture. This linear variation of $G_{pp}$ with filler content is reflected in our data for up to 4 wt % graphite flakes. The apparent decline in toughness with 5 wt % graphite requires confirmation, but might reflect the interaction of the higher stress fields around neighbouring flakes leading to matrix fracture before significant flake pullout.

Bone cements reinforced with hydroxyapatite particles also demonstrated an improvement in toughness, but the improvement was not as large as for the other reinforcing particles. With additions of 10 and 20 wt % the value of $K_{Ic}$ remained approximately constant at 1.23 MPa $m^{1/2}$. The fracture toughness increased further at 30 wt %, and attained 1.55 MPa $m^{1/2}$ at 40 wt %. Electron microscopy revealed no evidence of extensive plastic deformation on the fracture surfaces, so the toughening is probably due to pinning of the crack front by the filler particles. As the hydroxyapatite content was increased, the particle spacing was reduced, which resulted in greater energy absorption through Equation 3. The use of a silane coupling agent would improve interfacial bonding and probably yield a greater toughening effect.

Finally, it is important to note that the inherent porosity of the control specimens did not vary significantly through the addition of fillers. The composite bone cement with 40% DR100 had porosity values of 8.7 and 7.6%, whereas the control had comparable values of 7.8 and 7.9%. Although the depth of the database is admittedly small, it appears that the inclusion of fillers did not result in the formation of excess porosity.

## 4.2. The effect of fillers on curing

Reducing the peak curing temperature of bone cement is a desirable goal for several reasons: it minimizes thermal necrosis of adjacent tissues, it decreases the likelihood of vaporizing residual monomer to form pores and it provides for conditions that are suitable for forming a polymer with higher molecular weight and hence greater strength. The capability of filler materials to bring about the desired reduction in peak temperature has been documented in several studies of composite bone cements [15, 24, 25]. The results of the present investigation indicate that each of the fillers utilized effected a reduction in maximum curing temperature compared with the Zimmer LVC control.

The 4 wt % graphite and 6 wt % Paraloid KM334 composites gave reductions in peak temperature of 5.1 and 5.7 °C, respectively. However, the 40 wt % hydroxyapatite and 40 wt % Plexiglas DR100 composites resulted in greater temperature reductions, 7.2 and 8.2 °C, respectively. This can be related to the ability of the fillers to act as heat sinks, their performance being linked to both the filler content and the filler heat capacity.

The differential scanning calorimetry trials determined the heat capacity of the unmodified Zimmer LVC cement to be 1.59 J $g^{-1}$ $°C^{-1}$; a value of 1.46 was quoted by Huiskes *et al.* [26], but the type of bone cement was not specified. Both of the rubber modifiers exhibited heat capacities only slightly inferior to those of unmodified cement. This was to be expected, since all three materials are thermoplastic polymers. The heat capacity of the graphite and hydroxyapatite are very similar in magnitude, but only about half the value of the Zimmer cement. The capability of the fillers to reduce the curing temperature of the polymer dough relies on a combination of their mass and heat capacity, i.e. on the product $mC_p$. A direct relationship is evident between this heat sink value and the peak temperature for the various cements. As expected, the composites with the highest values of $mC_p$ developed the lowest maximum curing temperatures. The 40 wt % DR100 composite developed a peak temperature of 24.9 °C (versus 33 °C for Zimmer LVC alone), with a heat sink value of 0.174 J $°C^{-1}$. The highest curing temperature was generated by the 4 wt % graphite composite, which also possessed the lowest heat sink value. Clearly, the success of the DR100 cement can be attributed to the large mass content and high heat capacity of that filler.

Variations in the ratio PMMA powder/MMA liquid brought about by replacing significant amounts of the PMMA powder with the filler material can also

effect a change in the setting process. The incorporation of 4 wt % particulates transforms the PMMA powder/MMA liquid ratio from the intended 2:1 value to about 1.9:1, clearly not a significant alteration. However, 40 wt % filler reduces the ratio to 1.2:1.

This adjustment of the reactant content induces a change in the kinetics of the polymerization reaction. Reducing the powder/liquid ratio from 2:1 to 1.2:1 removes a portion of initiator that would otherwise be present in the PMMA powder. Furthermore, the greater amount of liquid constitutes a much larger reservoir of MMA monomer reactant units. In general, reducing the powder/liquid ratio results in a higher exothermic temperature and protracted setting time [27]. Consequently, the peak temperatures obtained by the composite cements could be reduced even further by tailoring the $P/L$ ratio to account for the loss of initiator. The lengthened setting times, especially for the 40 wt % hydroxyapatite and 6 wt % Paraloid composites, are grounds for serious concern regarding the clinical applicability of these materials. The surgeon must manually immobilize the implant while the cement sets to an extent that can adequately fix the implant in the required position. It is not realistic to expect that an implant can be held motionless for 20 min while a cement sets.

### 4.3. Workability

Even if a filler improves the toughness of a bone cement significantly, the cement is of limited use unless it can be introduced easily into the cavity between the implant and medullary canal. Vacancies or large pores in this region would be unacceptable because the reliability of the implant would almost certainly be compromised. A concern with the use of fibre-reinforced bone cement has been the deleterious effect of the high-aspect ratio fibres on the cement intrusion characteristics [28]. The use of particulate fillers appears to overcome this problem.

Both the 6 wt % Paraloid KM334 and the 4 wt % graphite composites exhibited workabilities only slightly inferior to those of the unmodified cement. For the KM334 composite, this can be related to the similarity in particle size between the filler and the PMMA powder. The unexpectedly high workability of the graphite flake-reinforced material is thought to be due to the sleek profile of the flakes and the low filler content.

The poor performance of the 40 wt % Plexiglas DR100 composite cement can be attributed to the large mean particle size and broad size distribution produced by the cryogenic grinding process. As a result, the success of this cement in an operating room environment is questionable. A more effective grinding procedure should be developed to reduce the mean particle size to a more acceptable level.

The 40 wt % hydroxyapatite cement displayed a workability greater than that of the Zimmer LVC control cement. Because a portion of the PMMA powder is replaced by the filler material, the mixing proportions result in an excess of MMA within the curing polymer dough. The excess MMA would have reduced the viscosity of the polymer and thereby improved the apparent workability.

### 4.4. Clinical use of composite cements

Although our tests have indicated an increase in fracture toughness results from incorporation of the fillers studied, further testing is necessary before clinical use of these cements. Fracture toughness is a measure of a material's intrinsic ability to resist unstable crack propagation. For a material such as bone cement in which internal voids and surface irregularities cannot be avoided during its *in situ* curing, resistance to unstable crack propagation is considered to be a more important characteristic than resistance to crack formation. Hence, during cyclic loading, crack propagation resistance will be a strong determinant of fatigue strength and lifetime-to-failure. However, fatigue testing *per se* is recommended to confirm this. Furthermore, our fracture toughness testing was limited to room-temperature, dry conditions at one strain rate only. Further testing at 37 °C in wet environments and at different loading rates is recommended.

Finally, as with all new materials for implant applications, assessment of the biocompatibility of these composite cements is necessary. Both tissue tolerance to the composites and the material response to prolonged *in vivo* exposure must be determined before clinical use.

## 5. Conclusions

The fracture toughness of a low-viscosity commercial bone cement was improved significantly by incorporating various particulate fillers. Plexiglas DR100 was the most effective toughening agent, increasing the $K_{Ic}$ of the cement from 1.07 to 2.08 MPa $m^{1/2}$ (at 40 wt %).

The filler particles were found to behave as heat sinks during setting, thereby reducing the peak temperature of the curing bone cement. Plexiglas DR100 resulted in the greatest reduction in the peak temperature, due in part to its heat capacity and large mass content.

Each of the fillers affected the intrusion characteristics of the polymer dough. The 40 wt% hydroxyapatite cement increased the workability relative to the unmodified low-viscosity cement, whereas 4 wt % graphite and 6 wt % Paraloid KM334 induced nominal reductions in workability. The cement modified with 40 wt % Plexiglas DR100 decreased the workability significantly, presumably due to the large particle size of this filler.

## References


1. W. KRAUSE and R. S. MATHIS, *J. Biomed. Mater. Res.* **22** (1988) 37.
2. R. N. STAUFFER, *J. Bone Joint Surg.* **64** (1982) 983.
3. C. J. HOOLEY, D. R. MOORE, M. WHALE and M. J. WILLIAMS, *Plast. Rubber Process. Applics* **1** (1981) 345.
4. A. D. SCHELLER and J. D'ERRICO, in "Revision total hip arthroplasty" (Grune and Stratton, New York, 1982) p. 49.
5. C. T. WANG and R. M. PILLIAR, *J. Mater. Sci.* **24** (1989) 2391.

6. *Idem, ibid.* **24** (1989) 3725.
7. L. M. BARKER, *Int. J. Fracture* **15** (1979) 515.
8. ASTM Standard F451-86, "1986 Annual book of ASTM standards", Vol. 13.01 (American Society of Testing and Materials, Philadelphia, 1986) p. 100.
9. T. WATSON, M. JOLLES, P. PEYSER and S. MOSTOVOY, *J. Mater. Sci.* **22** (1987) 1249.
10. R. P. ROBINSON, T. M. WRIGHT and A. H. BURNSTEIN, *J. Biomed. Mater. Res.* **15** (1981) 203.
11. B. POURDEYHIMI and H. D. WAGNER, *ibid.* **23** (1989) 63.
12. S. SAHA and S. PAL, *J. Biomech.* **17** (1984) 467.
13. T. M. WRIGHT and P. S. TRENT, *J. Mater. Sci.* **14** (1979) 503.
14. J. MILIOS *et al., ibid.* **21** (1986) 4281.
15. A. MURAKAMI, J. C. BEHIRI and W. BONFIELD, *ibid.* **23** (1988) 2029.
16. E. LAWRENCE and J. BROUTMAN (editors), in "Fracture and fatigue" (Academic Press, New York, 1974) p. 1.
17. M. KAWAGOE and M. KITAGAWA, *J. Mater. Sci.* **23** (1988) 3927.
18. R. N. HOWARD (editor), "The physics of glassy polymers" (Wiley, New York, 1973) p. 440.
19. Y. W. MAI and B. COTTERELL, *Int. J. Fracture* **32** (1986) 105.
20. C. B. BUCKNALL, in "Toughened plastics" (Applied Science, London, 1977) p. 100.
21. N. SHAH, *J. Mater. Sci.* **23** (1988) 3623.
22. C. V. S. KAMESWARA RAO, *Engng Fracture Mech.* **18** (1983) 35.
23. M. R. PIGGOTT, in "Load bearing fibre composites" (Pergamon Press, Toronto, 1980) p. 83.
24. A. CASTALDINI, A. CAVALLINI, A. MORONI and R. OLMI, in "Biomaterials and biomechanics" (Elsevier Science, Amsterdam, 1984) p. 427.
25. G. GUIDA, V. RICCIO, S. GATTO, C. MIGLIARESI, L. NICODEMO, L. NICOLAIS and C. PALOMBA, *ibid.* p. 19.
26. R. HUISKES *et al.*, in "Evaluation of biomaterials" (Wiley, Chichester, 1980) p. 189.
27. E. P. LAUTENSCHALGER *et al.*, in "Functional behaviour of orthopaedic biomaterials: applications" (CRC Press, Boca Raton, Florida, 1984) p. 88.
28. R. M. PILLIAR, R. BLACKWELL, I. MacNAB and H. U. CAMERON, *J. Biomed. Mater. Res.* **10** (1976) 983.
29. T. A. FREITAG and S. L. CANNAN, *ibid.* **10** (1976) 805.

*Received 25 May*
*and accepted 8 November 1991*